

Universal Approximation Theory: The Basic Theory for Deep Learning-Based Computer Vision Models

Wei Wang¹, Qing Li¹

¹The Hong Kong Polytechnic University

weiuat.wang@connect.polyu.hk, qing-prof.li@polyu.edu.hk

Abstract

Computer vision (CV) is one of the most crucial fields in artificial intelligence. In recent years, a variety of deep learning models based on convolution and Transformer have been designed to tackle diverse problems in CV. These algorithms have found practical applications in areas such as robotics and facial recognition. Despite the increasing power of current CV models, several fundamental questions remain unresolved: Why do convolutional neural networks (CNNs) require deep layers? What ensures the generalization ability of CNNs? Why do residual-based networks outperform fully convolutional networks like VGG? What is the fundamental difference between residual-based CNNs and Transformer-based networks? What are the differences between human vision and deep learning-based CVs? The root cause of these questions lies in the lack of a robust theoretical foundation for deep learning models in CV. To address these critical issues and techniques, we employ the Universal Approximation Theorem (UAT) to provide a theoretical basis for convolution- and Transformer-based models in CV. By doing so, we aim to elucidate these questions from a theoretical perspective.

1 Introduction

As a core branch of artificial intelligence, CV has a wide range of applications, encompassing tasks such as image segmentation (Minaee et al. 2021; Wang et al. 2022a), classification (Rawat and Wang 2017; Wang et al. 2017), video synthesis (Wang et al. 2018, 2019a), and restoration (Wang et al. 2019b; Nah et al. 2019). This broad applicability highlights its enormous technical potential and practical significance, making the intelligent processing of CV tasks a highly important area of research. The most effective solutions in this field today are based on deep learning algorithms.

One of the earliest and most influential works in using deep learning for CV was LeNet (Lecun et al. 1998), which pioneered the use of CNNs for handwritten digit recognition, ushering in a new era of image processing. Following this, AlexNet’s (Krizhevsky, Sutskever, and Hinton 2017) remarkable performance on the ImageNet (Russakovsky et al. 2014) dataset not only achieved a significant leap in image

classification accuracy but also cemented CNNs as the dominant method in visual processing. The subsequent introduction of ResNet (He et al. 2016) further improved image recognition accuracy and established residual-based structure as a foundational architecture for future network designs, influencing nearly all subsequent deep learning models (Ren et al. 2015; Xie et al. 2016; Szegedy et al. 2014; Gao et al. 2019; Liu et al. 2021).

In recent years, the success of Transformers (Vaswani et al. 2017) in the field of natural language processing (NLP) has gradually permeated CV. Researchers have begun designing models for CV based on Transformers, such as the Vision Transformer (ViT) (Dosovitskiy et al. 2020), Swin Transformer (Liu et al. 2021) and StructViT (Kim et al. 2024), which have demonstrated capabilities comparable to CNNs in image tasks (For convenience, we collectively refer to all Transformer-based models in the CV domain as ViTs.). Currently, research in deep learning for image processing predominantly revolves around CNNs (Huang et al. 2023; Wang et al. 2022b), Transformers (Shi 2023; Wang et al. 2023), or strategies that integrate both (Lv et al. 2023; Hou et al. 2024), continuously driving technological advancements.

Despite the significant advances in deep learning-based computer vision, several fundamental questions remain unanswered. For instance, why do convolutional neural networks (CNNs) require such deep architectures? What underpins the generalization ability of CNNs? Why do residual networks outperform fully convolutional networks like VGG (Simonyan and Zisserman 2014)? What are the core differences between residual-based CNNs and Transformer-based models? We believe that these questions arise from the lack of a foundational theory for CNNs.

While some researchers have attempted to explain CNNs through various approaches—such as using visualization techniques to analyze the relationship between feature maps and original images (Wei et al. 2016) or exploring CNNs from the frequency domain perspective (Yin et al. 2019; Xu, Zhang, and Xiao 2019)—these explanations often have limitations and are somewhat subjective. Similarly, studies on the interpretability of Vision Transformers (ViTs) (Park and Kim 2022; Bai et al. 2022) suggest that the multi-head attention (MHA) mechanism in Transformers tends to capture low-frequency information, in contrast to CNNs,

which function as high-pass filters. These studies advocate for combining the strengths of both models or improving ViTs to better capture high-frequency details. However, these methods only provide intuitive explanations for specific problems and fail to offer a theoretical framework for addressing broader issues within CNNs and ViTs. Essentially, they describe or interpret phenomena occurring within CNNs or ViTs rather than providing a comprehensive theory for these architectures.

To address these issues, we propose a unified explanation for the problems in CNNs and ViTs under the framework of the UAT. Although some previous works (Lin, Shen, and Li 2022; Yang, Feng, and Zhou 2024; Zhou 2018, 2020) have attempted to use UAT to explain certain aspects of CNNs, these studies are often limited to specific conditions and lack general applicability and practical guidance. For example, they fail to fundamentally explain the differences between residual-based CNNs and VGG, and they do not extend to ViT architectures. Our goal is to leverage the Matrix-Vector method introduced in UAT2LLMs (Wang and Li 2024b) to demonstrate that both CNNs and ViTs are concrete implementations of UAT and to theoretically resolve these issues in a way that can also provide practical guidance for network design (Wang and Li 2024a). Our contributions are as follows:

- We used the Matrix-Vector Method to demonstrate that the multi-layer convolutional and Transformer structures commonly employed in the field of CV are specific implementations of the UAT.
- We explained why CNNs require deep networks, considering the characteristics of image data and the UAT model perspective.
- We proved why the widely used residual structure in CV is so powerful.
- We compared multi-layer convolutional residual structures and Transformer structures from the UAT perspective, illustrating the source of their powerful capabilities and explaining why both models appear to have similar performance.
- we provided a comparison between human vision and deep learning-based CV.

The structure of this paper is as follows: In Section 2, we introduce the UAT and the Matrix-Vector Method, as well as their relationship. In Section 3, we use the Matrix-Vector Method to transform some commonly used operations in CV into matrix-vector forms, such as 2D convolution (3.1), 3D convolution (3.2), mean-pooling (3.3), and Transformer (3.4). In Section 4, we address some fundamental questions in CV: why CNN networks need to be deep (4.1), why residual-based CNNs are more powerful than VGG (4.2), the differences between residual-based CNNs and Transformer-based networks (4.3), and the relationship between human vision and deep learning-based CV(4.4).

2 UAT for CV

We have previously introduced our goal of unifying CNNs and ViTs in the field of CV under the framework of UAT. Using UAT, we aim to explain existing problems in CV. So we

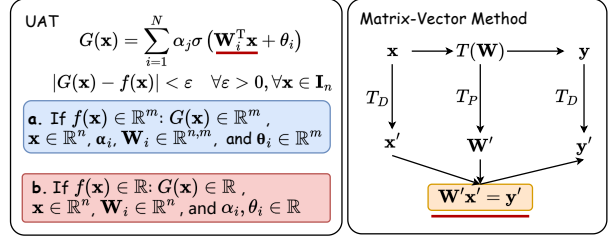


Figure 1: The basic format of UAT and The Matrix-Vector Method and their relationship.

will follow the UAT2LLMs' (Wang and Li 2024b) thoughts to leverage the Matrix-Vector Method to unify CNNs and ViTs under the UAT framework. Before formally unifying CNNs and ViTs within UAT, we will briefly introduce the Matrix-Vector Method and the unification approach proposed in UAT2LLMs.

Figure 1 simply outlines the proof route in UAT2LLMs: first, $G(\mathbf{x})$ represents the general form of UAT, capable of approximating Borel measurable functions within a closed interval(Cybenko 2007; Hornik, Stinchcombe, and White 1989), where I_n denotes an n-dimensional unit cube. UAT includes one-dimensional and high-dimensional approximations, corresponding to Figures 1.a and 1.b, respectively. It is evident that the basic UAT computing unit is $\alpha_j \sigma(\mathbf{W}_j^T \mathbf{x} + \theta_j)$. $\mathbf{W}_j^T \mathbf{x} + \theta_j$ can be seen as operations of convolution and mean pooling in CNNs, and MHA and linear in ViTs. Therefore, if we can transform these operations into a matrix multiplying a vector using the Matrix-Vector Method in Figures 1 (Details could be seen in UAT2LLMs), it becomes straightforward to prove that multi-layer CNNs and ViTs are specific implementations of UAT.

The Matrix-Vector Method is illustrated in Figure 1, where T denotes various transformations in CNNs and ViTs, and T_D and T_P represent specific transformation methods. These transformations convert the input data \mathbf{x} and output data \mathbf{y} , along with parameters \mathbf{W} , into vectors \mathbf{x}' and \mathbf{y}' , and parameter matrices \mathbf{W}' , satisfying the computational requirements shown in the Figure 1. To distinguish them from the original variables, we will add a ' symbol to the upper right of the original variables, indicating their corresponding matrix-vector form. (Note: The key challenge is converting them into matrix-vector form, so bias terms are omitted here.)

Additionally, due to the complexity of convolution and Transformer calculations, a computational tool called diamond matrix multiplication has been designed to clearly elucidate the process of converting convolution or Transformer operations into their corresponding matrix-vector representations. Its relationship with standard matrix multiplication is $\mathbf{W} \diamond \mathbf{x} = \mathbf{W}^T \mathbf{x}$. The diamond matrix enhances the clarity of this conversion process. (The details and properties can be found in UAT2LLMs.)

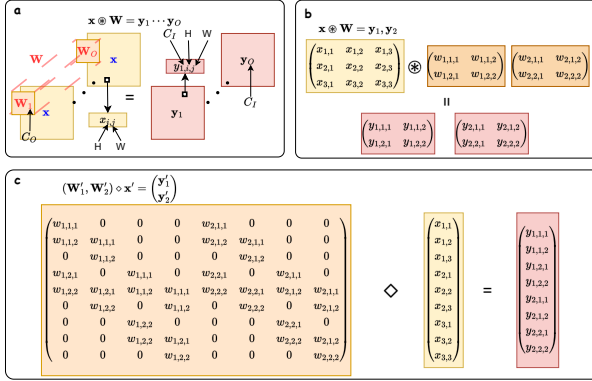


Figure 2: 1-O Conv2D process and the matrix-vector transformation example. In **a**, we present the operation of 1-O Conv2D. At the top of **a**, **b** and **c**, we provide the mathematical formula corresponding to the diagram. Additionally, we group the variables in the figure, such as $\mathbf{W} = \text{Concat}(\mathbf{W}_1, \dots, \mathbf{W}_O)$. In **b**, we provide an example corresponding to **a**, and in **c**, we show the matrix-vector form of the example given in **b**. The following figures follow the same conventions.

3 The Matrix-Vector Method for CNNs and ViTs

In the previous sections, we explained that to unify CNNs and ViTs under the UAT, it is necessary to demonstrate that their various transformations (convolution, mean pooling, MHA, and linear) can be represented in matrix-vector form. UAT2LLMs has already shown how to represent MHA and linear in matrix-vector form. Therefore, in this section, we will specifically demonstrate how to convert convolution and mean pooling in CNNs into matrix-vector form using the Matrix-Vector Method. Additionally, we will interpret the unique aspects of MHA in ViTs within the context of CV.

Considering that convolution in CV can be either 2D or 3D and that the input and output may consist of single or multiple channels. We use the notation 1 to represent a single channel, I to represent an input with I channels, and O to represent an output with O channels. For example, 1-O indicates an operation with one channel input and O channels output. Below, we will show how to convert these transformations into the corresponding matrix-vector forms.

3.1 The Matrix-Vector Method for Conv2D

In this section, we will detail how to convert 2D convolution into its corresponding matrix-vector forms, focusing on two scenarios: 1-O and I-O. To clearly describe the 2D convolution process, we first outline the general procedure and some basic conventions. The general process of 2D convolution involves convolving a kernel with the input data and then summing along the input channel direction (referred to as the C_I direction) to obtain an element in the output. The convolution kernel slides along the height (H) and width (W) directions to produce the entire output feature map. To generate multiple feature maps, multiple sets of convolution

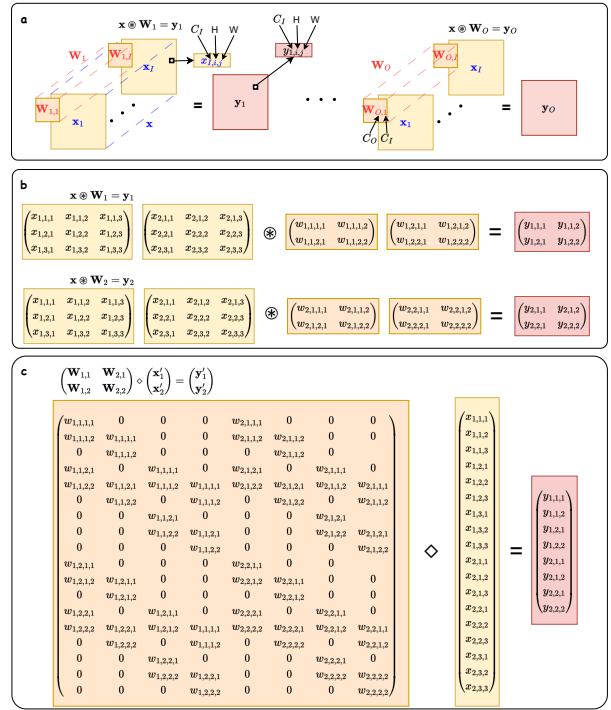


Figure 3: I-O Conv2D process and the matrix-vector transformation example.

kernels, C_O , are required, with each set having the same number of channels as the input channels. Depending on the context, C_I , C_O , H , and W can represent either the corresponding dimension directions or the number of dimensions in those directions. Figures 2 and 3 illustrate the conversion process for the cases of 1-O and I-O, transforming them into matrix-vector representations.

Specifically, Figure 2.a shows the process of 1-O Conv2D. Here, $\mathbf{W}_1 \dots \mathbf{W}_O$ represent the convolution kernels, which slide across the input data along the H and W directions. For a single-channel input producing O channels output, O convolution kernels convolve with the same input \mathbf{x} to produce outputs $\mathbf{y}_1 \dots \mathbf{y}_O$. Figure 2.b provides an example of a 1-O Conv2D. Additionally, Figure 2.c further converts the example given in Figure 2.b into its corresponding matrix-vector form. Therefore, it is straightforward to derive the matrix-vector form of 1-O Conv2D as follows:

$$(\mathbf{W}'_1 \quad \mathbf{W}'_2 \quad \dots \quad \mathbf{W}'_O) \diamond \mathbf{x}' = \begin{pmatrix} \mathbf{y}'_1 \\ \mathbf{y}'_2 \\ \vdots \\ \mathbf{y}'_O \end{pmatrix} \quad (1)$$

Figure 3.a depicts the general process of I-O Conv2D, considering the scenario with I channels input and O channels output. This requires O sets of convolution kernels, each set containing I kernels, collectively represented as $\mathbf{W}_{1,1} \dots \mathbf{W}_{1,I} \dots \mathbf{W}_{O,1} \dots \mathbf{W}_{O,I}$. Each kernel $\mathbf{W}_{i,j}$ with indices i, j convolves with the j -th input channel \mathbf{x}_j to produce an intermediate output $\mathbf{y}_{i,j}$. Summing all intermediate

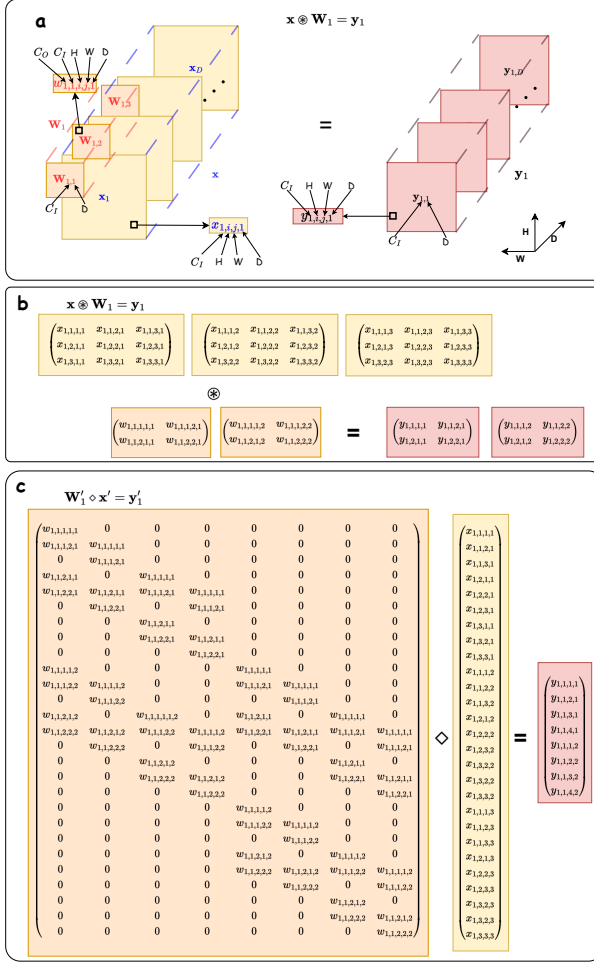


Figure 4: 1-O Conv3D process and the matrix-vector transformation example.

outputs $y_{i,1} \cdots y_{i,I}$ in the i -th set yields the final i -th output channel y_i . Figure 3.b provides a simplified example. Subsequently, Figure 3.c presents the corresponding matrix-vector representation for the example in Figure 3.b. Therefore, the matrix-vector formula for I-O Conv2D can be expressed as follows:

$$\begin{pmatrix} \mathbf{W}'_{1,1} & \mathbf{W}'_{2,1} & \cdots & \mathbf{W}'_{O,1} \\ \mathbf{W}'_{1,2} & \mathbf{W}'_{2,2} & \cdots & \mathbf{W}'_{O,2} \\ \vdots & \vdots & \vdots & \vdots \\ \mathbf{W}'_{1,I} & \mathbf{W}'_{2,I} & \cdots & \mathbf{W}'_{O,I} \end{pmatrix} \diamond \begin{pmatrix} \mathbf{x}'_1 \\ \mathbf{x}'_2 \\ \vdots \\ \mathbf{x}'_I \end{pmatrix} = \begin{pmatrix} \mathbf{y}'_1 \\ \mathbf{y}'_2 \\ \vdots \\ \mathbf{y}'_O \end{pmatrix} \quad (2)$$

3.2 The Matrix-Vector Method for Conv3D

3D convolution is a structure designed primarily for video or 3D image data, consisting mainly of two forms: 1-O Conv3D and I-O Conv3D. Given their complexity, we provide proof examples only for the 1-1 and I-1 Conv3D forms. The forms of 1-O and I-O Conv3D can be easily derived from the 1-1 and I-1 Conv3D forms. Compared with 2D convolution, 3D convolution has an additional depth dimension (D). So the convolution kernel could slide along with H, W, D , and it also needs to sum in C_I direction.

Figure 4 illustrates the process of converting 1-1 Conv3D into its matrix-vector form. Figure 4.a shows the general form of 1-O Conv3D. As a 3D convolution, the input data typically has four dimensions: (C_I, H, W, D) , representing the number of input channels, height, width, and depth, respectively. In 1-1 Conv3D, C_I equal to 1. The convolution kernel has an additional dimension C_O , representing the number of output channels, and in this case, $C_O = 1$. The convolution kernel slides along the width (W), height (H), and depth (D) directions. Figure 4.b presents a specific example, while Figure 4.c converts this example into its matrix-vector form (ignoring changes in H, W, D dimensions due to lack of padding).

According to Figure 4, the matrix-vector form of 1-O Conv3D can be easily derived and is consistent with Eq. (1). The difference lies in the fact that \mathbf{W}_i has depth, so the corresponding \mathbf{W}'_i needs to be recombined as shown in Figure 4.c.

Similarly, Figures 5.a, b, and c illustrate the general process, a simple example, and the corresponding matrix-vector form of I-1 Conv3D, respectively. According to Figure 5, the matrix-vector form of I-O Conv3D is consistent with Eq. (2). The difference is that both \mathbf{x}_i and \mathbf{W}_i have depth, so the corresponding \mathbf{x}'_i and \mathbf{W}'_i need to be obtained as shown in Figure 5.c.

3.3 The Matrix-Vector Method for Mean Pooling

Mean pooling is also an important technique in the field of CV, often used in conjunction with convolution. To demonstrate that CNNs can be expressed in the form of UAT, we need to prove that mean pooling can also be represented in matrix-vector form. In Figure 6, we provide an example. Figure 6.a shows the process of mean pooling, while Figure 6.b illustrates its corresponding matrix-vector form. Based on Figure 6, we can conclude that mean pooling can indeed be represented in matrix-vector form.

3.4 Transformer for CV

In UAT2LLMs, it has been demonstrated that the feed-forward network (FFN) and MHA components in the Transformer architecture can be represented in matrix-vector form. Given that ViTs are also based on the Transformer framework, we only need to focus on the differences between Transformers in CV and those in UAT2LLMs. A key feature of ViTs is that they divide the original image into multiple patches: $\mathbf{x}_{1,1}, \dots, \mathbf{x}_{n,m}$. Each image patch is then reshaped into row vectors $\bar{\mathbf{x}}_{1,1}, \dots, \bar{\mathbf{x}}_{n,m}$, which are concatenated along the column direction to obtain $\tilde{\mathbf{x}}$, as shown in Figure 7. MHA and FFN operations are then applied, so aside from the initial processing part, the subsequent transformation process completely follows the description in UAT2LLMs. Therefore, it is easy to deduce that ViTs are also specific implementations of the UAT.

3.5 Summary

We know that various modules in CV, including 2D convolution, 3D convolution, mean pooling, MHA, and linear,

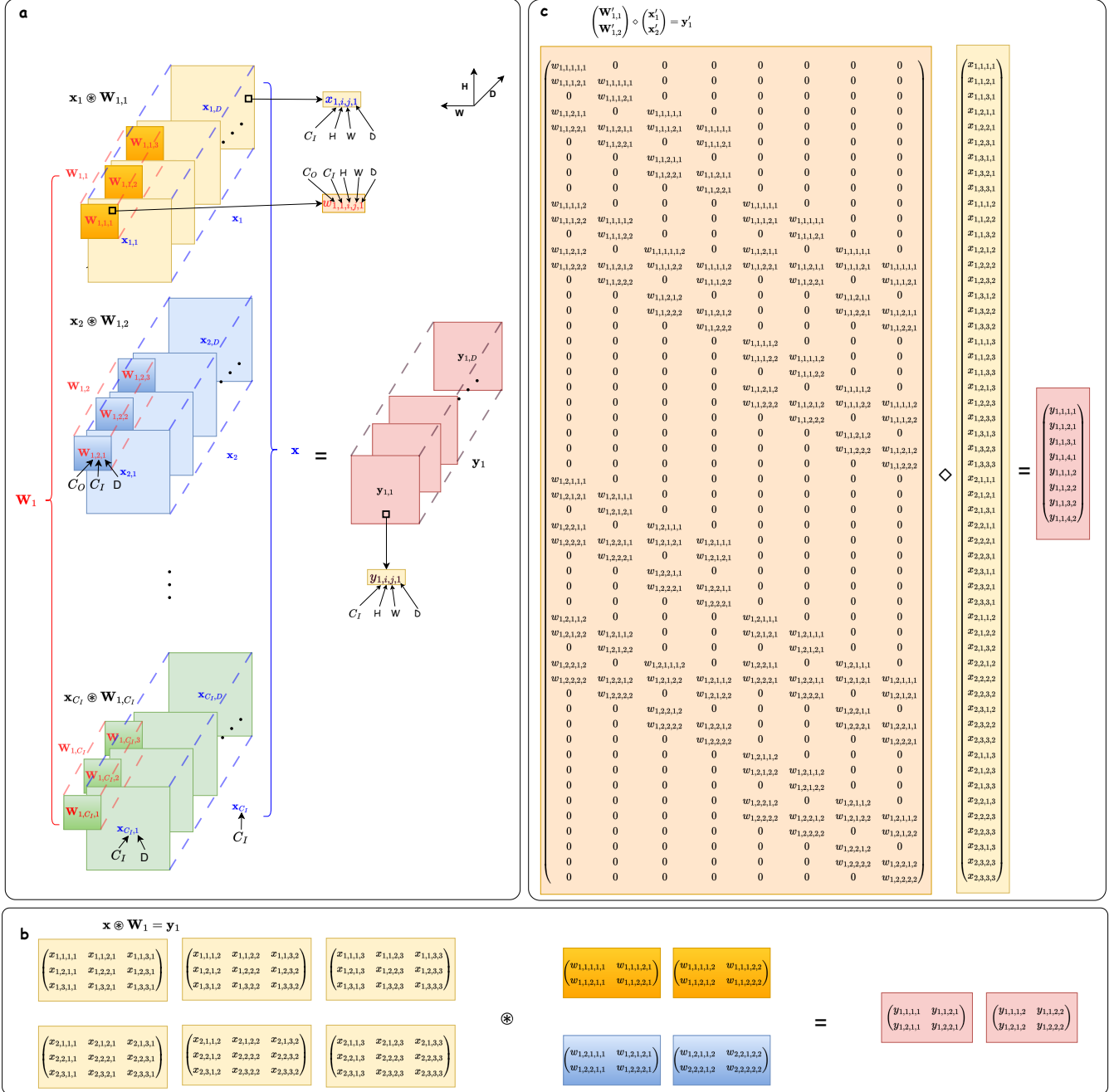


Figure 5: I-1 Conv3D process and the matrix-vector transformation example.

can all be represented by diamond matrix multiplication. Considering the relationship between diamond matrix multiplication and matrix multiplication: $\mathbf{W} \diamond \mathbf{x} = \mathbf{W}^T \mathbf{x}$. Therefore, unless otherwise specified, we will conveniently use $\mathbf{W}'\mathbf{x}'$ to represent the matrix-vector form of them. Here, \mathbf{W}' is derived from the parameters \mathbf{W} of the various modules, and \mathbf{x}' is derived from the inputs \mathbf{x} of the modules.

4 Discussion

In this section, we will answer the questions in the field of CV proposed in the Introduction.

4.1 Why must CNNs be Deep?

There are two main reasons why CNNs typically have deep layers. The first reason stems from the learning paradigm of CNNs. The design of CNNs is based on two well-known principles: local receptive fields (i.e., local features in images often contain important information) and

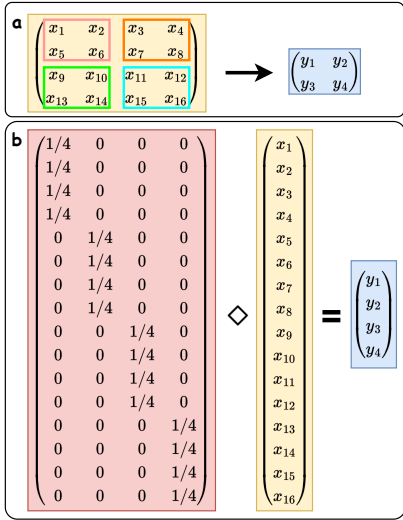


Figure 6: Mean pooling process and the matrix-vector transformation example. Pink, orange, green and blue boxes represent mean pooling size.

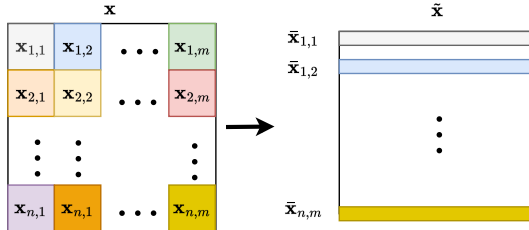


Figure 7: The MHA operation in CV.

spatial invariance (these important local features can appear anywhere in the image). These principles necessitate learning from each small region of the image, with all small regions sharing the same parameters. If parameters differed, it would imply that a certain object must appear in a specific part of the image, which is clearly unreasonable.

The above reasons dictate that image learning occurs in small patches, which explains why convolutional kernels are typically small. However, if the network has only a few layers, such as a single layer, it means that each small patch is learned independently. We know that objects in an image are generally composed of multiple such patches. Observing only a part of the image cannot provide a clear identification of the object. Therefore, a larger receptive field is needed, which can be achieved by increasing the number of layers to gather global information.

The second reason is derived from the UAT. As shown in Figure 1, increasing the number of layers in the network means a larger N , which brings the UAT closer to approximating the target function. An image can be understood as a special function in a high-dimensional space, exhibiting strong correlations in 2D or 3D space. These two reasons are also applicable to ViTs. Figure 7 shows the preprocessing of ViTs, where \tilde{x} is the input to the ViTs. It is evident

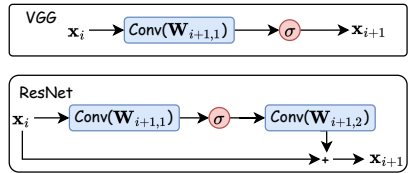


Figure 8: VGG Vs ResNet: The characters in '()' represent the corresponding operation's parameters. Hereinafter the same.

that each row shares the same parameters, and the learning of each row adheres to the principles of local receptive fields and spatial invariance.

4.2 Why Residual-Based CNNs Excel in CV: Superior Generalization Ability

In the previous discussion, we explained why deep networks are essential for learning in CNNs. However, why did VGG, despite being a deep network, not dominate the subsequent development of CV, whereas residual-based CNNs did? ResNet significantly shaped the design of later network architectures, with the residual structure appearing in many subsequent networks. What exactly endows the residual structure with such powerful capabilities? We think the answer is the generalization capability given by residual structure. To analyze the source of this power, we use the Matrix-Vector Method to express VGG and the residual structure in equations, and then compare them with the UAT.

Figure 8 illustrates the basic structures of VGG and ResNet. Based on this figure, a i -layer VGG can be written as:

$$\mathbf{x}'_i = \sigma\{\mathbf{W}'_i \cdots \sigma\{\mathbf{W}'_3[\sigma(\mathbf{W}'_2\sigma(\mathbf{W}'_1\mathbf{x}'_1 + \mathbf{b}'_1) + \mathbf{b}'_2)] + \mathbf{b}'_3\} + \mathbf{b}'_i\} \quad (3)$$

which perfectly aligns with the multilayer UAT mathematical form proposed by Hornik (Hornik, Stinchcombe, and White 1989). On the other hand, a multi-layer residual-based CNN can be expressed as:

$$\mathbf{x}'_{i+1} = (\mathbf{x}'_0 + \mathbf{b}'_{i+1,2}) + \sum_{j=1}^{i+1} \mathbf{W}'_{j,2} \sigma(\mathbf{W}'_{j,1}\mathbf{x}'_0 + \mathbf{b}'_{j,1}) \quad (4)$$

where $\mathbf{b}'_{j,1} = (\mathbf{W}'_{j,1}\mathbf{b}'_{j-1,2} + \mathbf{b}'_{j,1}) + \mathbf{W}'_{j,1}UAT_{j-1}^R$ and $UAT_{j-1}^R = \sum_{k=1}^{j-1} \mathbf{W}'_{k,2} \sigma(\mathbf{W}'_{k,1}\mathbf{x}'_0 + \mathbf{b}'_{k,1})$ (see Appendix A.2 for detail). Eq. (4) conforming to the UAT form given in Figure 1. In this equation, $\mathbf{b}'_{j,1}$ is a dynamic parameter approximated by j layers UAT ($j > 1$). It is evident that both VGG and ResNet are concrete implementations of UAT. Theoretically, their approximation capabilities should be equivalent, and any differences could be mitigated by increasing the number of network layers. So why is ResNet significantly more powerful than VGG?

The primary reason lies in the dynamic approximation capabilities of residual networks. As seen in Eq. (3), once a VGG network is trained, its corresponding UAT parameters

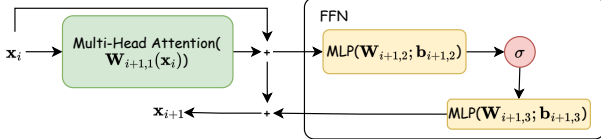


Figure 9: The process of Transformer.

are fixed. This means that a VGG network can only approximate a single, fixed function. Although UAT has strong approximation abilities, image data is highly variable, and the corresponding function often changes. In contrast, residual networks can dynamically approximate the corresponding function based on the input because the biases in residual networks are influenced by the input.

Therefore, while the original UAT formula has strong approximation capabilities, using it for approximation (equivalent to using a VGG network in CV) means that once training is complete, the UAT parameters are fixed, and the function it can approximate is also fixed. In contrast, in residual networks, the UAT parameters can change based on the input, allowing the function being approximated to vary accordingly. This adaptability is the fundamental source of the superiority of residual networks.

4.3 The Difference between Residual-Based CNNs and ViTs

In this section, we will compare the UAT format of Transformer-based ViTs and residual-based CNNs. Figure 9 shows the general form of a Transformer. A multi-layer Transformer can be expressed as:

$$\mathbf{x}_{i+1} = (\mathbf{W}'_{i+1,1}\mathbf{x}_0 + \mathbf{b}_{i+1,1}) + \sum_{j=1}^{i+1} \mathbf{W}'_{j,3} \sigma(\mathbf{W}'_{j,2}\mathbf{x}'_0 + \mathbf{b}'_{j,2}) \quad (5)$$

where $\mathbf{b}'_{j,2} = (\mathbf{W}'_{j,2}\mathbf{b}'_{j-1,3} + \mathbf{b}'_{j,2}) + \mathbf{W}'_{j,2}UAT_{j-1}^R$ and $UAT_{j-1}^R = \sum_{k=1}^{j-1} \mathbf{W}'_{k,3} \sigma(\mathbf{W}'_{k,2}\mathbf{x}'_0 + \mathbf{b}'_{k,2})$ (see [Appendix A.3](#) for details). The mathematical representation of ViT also conforms to UAT, with $\mathbf{b}'_{j,2}(j > 1)$ is approximated by j -layer UAT. The biggest difference between Transformers and residual-based CNNs lies in the parameters in the MHA mechanism dynamically changing with the input. Therefore, in the corresponding UAT mathematical form for Transformers, all $\mathbf{W}'_{i,1}$, $\mathbf{W}'_{j,1}$ and $\mathbf{W}'_{j,2}$ parameters for the i -th layer, where $j = 1, \dots, i$, are dynamically changing with the input.

The main difference between Transformer networks and residual-based multi-layer convolutional networks lies in how the input affects their corresponding UAT parameters. In Transformer networks, input information influences both weight and bias in the corresponding UAT. In contrast, in networks constructed with multiple residual convolutions, input information only influences bias in the corresponding UAT. Essentially, both types of networks have the ability to dynamically approximate functions based on input. This aligns with their nearly identical performance in the field of

CV, supporting the theoretical foundation that both are specific implementations of UAT capable of dynamically approximating the corresponding functions based on input.

4.4 Human Vision vs UAT Vision

Based on the above discussion, we can consider that deep learning-based CV models are implementations of UAT, which we refer to as UAT vision. So, what is the relationship between human vision and UAT vision? We believe that the human brain functions as a large network composed of one or multiple UATs. Because first neural network is perceptron (Rosenblatt 1963) which was designed based on the brain neuron. The Transformer and residual-based CNNs can also be understood as implementations of UAT, and the perceptron can be seen as a special form of UAT. Therefore, the concepts of memory and understanding, as defined by humans, do not fundamentally exist; rather, they can be categorized as reasoning based on the UAT in our brains. Just as deep vision networks do not have a database storing images, they directly approximate the corresponding results from the inputs (which can be simplified as $y = UAT(x)$). Specifically, humans and animals are born with certain weights in their brains, which are innate reflexes, such as infants instinctively knowing how to suckle. However, other weights in the brain need to be learned, and our process of observing the world from a young age is essentially a process of training these weights. Given that the eyes' vision operates at 30 frames per second (Lu et al. 2017), the brain would be trained on hundreds of millions of high-resolution images over a year.

So, what is human memory? We believe it is the ability to generate corresponding results based on inputs and the weights learned by the brain. The so-called memory always has an anchor point that triggers it, i.e., something that evokes the memory. For example, an object might remind us of childhood memories because the visual input is similar or identical to what we saw in our childhood. We then derive a memory image, which is input back into the brain, and iterated repeatedly until the entire memory fragment is formed. Memory bias occurs when the brain's weight parameters are updated, leading to different results from the same input. Since the brain's weights are trained based on the natural world, it only infers results that are reasonable within the realm of cognition. This is why it is challenging for us to imagine things that do not exist, as the weights related to images in our brains are trained based on the natural world.

5 Conclusion

This paper delves into the theoretical foundations of deep learning in the field of CV. Specifically, the current CV landscape is primarily dominated by CNNs and Transformer models. We utilize the Matrix-Vector Method to unify these models under the framework of the UAT. Based on this framework, we provide explanations for several common issues and techniques in CV. The requirement for deep networks in CNNs is jointly determined by the intrinsic characteristics of image data and the demands of UAT theory. The

robust generalization ability of residual networks stems from their ingenious design, which enables UAT to dynamically adapt to corresponding functions based on input data. Similarly, Transformer-based models possess this ability, with the key difference lying in which parameters of UAT they influence. Residual networks primarily affect the bias term, while Transformers influence both the weights and the bias. Additionally, we think the thinking process of humans in images is the same as UAT, they all use pre-trained parameters to fit the output. But the human brain is a more complex UAT system and it is on training all the time.

References

Bai, J.; Yuan, L.; Xia, S.-T.; Yan, S.; Li, Z.; and Liu, W. 2022. Improving vision transformers by revisiting high-frequency components. In *European Conference on Computer Vision*, 1–18. Springer.

Cybenko, G. 2007. Approximation by superpositions of a sigmoidal function. *Mathematics of Control, Signals, and Systems*, 303–314.

Dosovitskiy, A.; Beyer, L.; Kolesnikov, A.; Weissenborn, D.; Zhai, X.; Unterthiner, T.; Dehghani, M.; Minderer, M.; Heigold, G.; Gelly, S.; et al. 2020. An image is worth 16x16 words: Transformers for image recognition at scale. *arXiv preprint arXiv:2010.11929*.

Gao, S.; Cheng, M.-M.; Zhao, K.; Zhang, X.; Yang, M.-H.; and Torr, P. H. S. 2019. Res2Net: A New Multi-Scale Backbone Architecture. *IEEE Transactions on Pattern Analysis and Machine Intelligence*, 43: 652–662.

He, K.; Zhang, X.; Ren, S.; and Sun, J. 2016. Deep residual learning for image recognition. In *Proceedings of the IEEE conference on computer vision and pattern recognition*, 770–778.

Hornik, K.; Stinchcombe, M. B.; and White, H. L. 1989. Multilayer feedforward networks are universal approximators. *Neural Networks*, 2: 359–366.

Hou, X.; Liu, M.; Zhang, S.; Wei, P.; and Chen, B. 2024. Salience DETR: Enhancing Detection Transformer with Hierarchical Salience Filtering Refinement. *ArXiv*, abs/2403.16131.

Huang, T.; Yin, L.; Zhang, Z. A.; Shen, L.; Fang, M.; Pechenizkiy, M.; Wang, Z.; and Liu, S. 2023. Are Large Kernels Better Teachers than Transformers for ConvNets? In *International Conference on Machine Learning*.

Kim, M.; Seo, P. H.; Schmid, C.; and Cho, M. 2024. Learning Correlation Structures for Vision Transformers. *ArXiv*, abs/2404.03924.

Krizhevsky, A.; Sutskever, I.; and Hinton, G. E. 2017. ImageNet classification with deep convolutional neural networks. *Commun. ACM*, 60(6): 84–90.

Lecun, Y.; Bottou, L.; Bengio, Y.; and Haffner, P. 1998. Gradient-based learning applied to document recognition. *Proceedings of the IEEE*, 86(11): 2278–2324.

Lin, T.-W.; Shen, Z.; and Li, Q. 2022. On the Universal Approximation Property of Deep Fully Convolutional Neural Networks. *ArXiv*, abs/2211.14047.

Liu, Z.; Lin, Y.; Cao, Y.; Hu, H.; Wei, Y.; Zhang, Z.; Lin, S.; and Guo, B. 2021. Swin Transformer: Hierarchical Vision Transformer using Shifted Windows. *2021 IEEE/CVF International Conference on Computer Vision (ICCV)*, 9992–10002.

Lu, J.; Gu, B.; Wang, X.; and Zhang, Y. 2017. High-speed adaptive optics line scan confocal retinal imaging for human eye. *PloS one*, 12(3): e0169358.

Lv, W.; Xu, S.; Zhao, Y.; Wang, G.; Wei, J.; Cui, C.; Du, Y.; Dang, Q.; and Liu, Y. 2023. DETRs Beat YOLOs on Real-time Object Detection. *ArXiv*, abs/2304.08069.

Minaee, S.; Boykov, Y.; Porikli, F.; Plaza, A.; Kehtarnavaz, N.; and Terzopoulos, D. 2021. Image segmentation using deep learning: A survey. *IEEE transactions on pattern analysis and machine intelligence*, 44(7): 3523–3542.

Nah, S.; Baik, S.; Hong, S.; Moon, G.; Son, S.; Timofte, R.; and Mu Lee, K. 2019. Ntire 2019 challenge on video deblurring and super-resolution: Dataset and study. In *Proceedings of the IEEE/CVF conference on computer vision and pattern recognition workshops*, 0–0.

Park, N.; and Kim, S. 2022. How do vision transformers work? *arXiv preprint arXiv:2202.06709*.

Rawat, W.; and Wang, Z. 2017. Deep convolutional neural networks for image classification: A comprehensive review. *Neural computation*, 29(9): 2352–2449.

Ren, S.; He, K.; Girshick, R. B.; and Sun, J. 2015. Faster R-CNN: Towards Real-Time Object Detection with Region Proposal Networks. *IEEE Transactions on Pattern Analysis and Machine Intelligence*, 39: 1137–1149.

Rosenblatt, F. 1963. PRINCIPLES OF NEURODYNAMICS. PERCEPTRONS AND THE THEORY OF BRAIN MECHANISMS. *American Journal of Psychology*, 76: 705.

Russakovsky, O.; Deng, J.; Su, H.; Krause, J.; Satheesh, S.; Ma, S.; Huang, Z.; Karpathy, A.; Khosla, A.; Bernstein, M. S.; Berg, A. C.; and Fei-Fei, L. 2014. ImageNet Large Scale Visual Recognition Challenge. *International Journal of Computer Vision*, 115: 211 – 252.

Shi, D. 2023. TransNeXt: Robust Foveal Visual Perception for Vision Transformers. *ArXiv*, abs/2311.17132.

Simonyan, K.; and Zisserman, A. 2014. Very Deep Convolutional Networks for Large-Scale Image Recognition. *CoRR*, abs/1409.1556.

Szegedy, C.; Liu, W.; Jia, Y.; Sermanet, P.; Reed, S. E.; Anguelov, D.; Erhan, D.; Vanhoucke, V.; and Rabinovich, A. 2014. Going deeper with convolutions. *2015 IEEE Conference on Computer Vision and Pattern Recognition (CVPR)*, 1–9.

Vaswani, A.; Shazeer, N. M.; Parmar, N.; Uszkoreit, J.; Jones, L.; Gomez, A. N.; Kaiser, L.; and Polosukhin, I. 2017. Attention is All you Need. In *Neural Information Processing Systems*.

Wang, A.; Chen, H.; Lin, Z.; Pu, H.; and Ding, G. 2023. RepViT: Revisiting Mobile CNN From ViT Perspective. *ArXiv*, abs/2307.09283.

Wang, F.; Jiang, M.; Qian, C.; Yang, S.; Li, C.; Zhang, H.; Wang, X.; and Tang, X. 2017. Residual attention network for image classification. In *Proceedings of the IEEE conference on computer vision and pattern recognition*, 3156–3164.

Wang, R.; Lei, T.; Cui, R.; Zhang, B.; Meng, H.; and Nandi, A. K. 2022a. Medical image segmentation using deep learning: A survey. *IET Image Processing*, 16(5): 1243–1267.

Wang, T.-C.; Liu, M.-Y.; Tao, A.; Liu, G.; Kautz, J.; and Catanzaro, B. 2019a. Few-shot video-to-video synthesis. *arXiv preprint arXiv:1910.12713*.

Wang, T.-C.; Liu, M.-Y.; Zhu, J.-Y.; Liu, G.; Tao, A.; Kautz, J.; and Catanzaro, B. 2018. Video-to-video synthesis. *arXiv preprint arXiv:1808.06601*.

Wang, W.; and Li, Q. 2024a. Universal Approximation Theory: Foundations for Parallelism in Neural Networks. *arXiv*:2407.21670.

Wang, W.; and Li, Q. 2024b. Universal Approximation Theory: The basic theory for large language models. *arXiv*:2407.00958.

Wang, X.; Chan, K. C.; Yu, K.; Dong, C.; and Change Loy, C. 2019b. Edvr: Video restoration with enhanced deformable convolutional networks. In *Proceedings of the IEEE/CVF conference on computer vision and pattern recognition workshops*, 0–0.

Wang, Z.; Bai, Y.; Zhou, Y.; and Xie, C. 2022b. Can CNNs Be More Robust Than Transformers? *ArXiv*, abs/2206.03452.

Wei, X.-S.; Luo, J.-H.; Wu, J.; and Zhou, Z.-H. 2016. Selective Convolutional Descriptor Aggregation for Fine-Grained Image Retrieval. *IEEE Transactions on Image Processing*, 26: 2868–2881.

Xie, S.; Girshick, R. B.; Dollár, P.; Tu, Z.; and He, K. 2016. Aggregated Residual Transformations for Deep Neural Networks. *2017 IEEE Conference on Computer Vision and Pattern Recognition (CVPR)*, 5987–5995.

Xu, Z.-Q. J.; Zhang, Y.; and Xiao, Y. 2019. Training behavior of deep neural network in frequency domain. In *Neural Information Processing: 26th International Conference, ICONIP 2019, Sydney, NSW, Australia, December 12–15, 2019, Proceedings, Part I* 26, 264–274. Springer.

Yang, Y.; Feng, H.; and Zhou, D.-X. 2024. On the rates of convergence for learning with convolutional neural networks. *ArXiv*, abs/2403.16459.

Yin, D.; Gontijo Lopes, R.; Shlens, J.; Cubuk, E. D.; and Gilmer, J. 2019. A fourier perspective on model robustness in computer vision. *Advances in Neural Information Processing Systems*, 32.

Zhou, D.-X. 2018. Universality of Deep Convolutional Neural Networks. *ArXiv*, abs/1805.10769.

Zhou, D.-X. 2020. Theory of deep convolutional neural networks: Downsampling. *Neural networks : the official journal of the International Neural Network Society*, 124: 319–327.

A The UAT Format of Residual-based CNNs and Transformer-based ViTs

Note: The sections A.1 and A.3 have already been proven in UAT2LLMs. For completeness, we also include them in this paper.

In this section, we will use the matrix-vector method to demonstrate the mathematical forms of residual-based CNNs and Transformer-based ViTs, and their relationship with UAT. In Section A.1, we first presented some lemmas of UAT. Using these lemmas, we then proved that residual-based CNNs A.2 and Transformer-based ViTs A.3 are specific implementations of UAT.

A.1 The Properties of UAT

Before expressing CNNs based on residuals and Transformers based on ViTs in the UAT format, we present two lemma regarding UAT. There are two cases for UAT-approximated functions: $f(\mathbf{x}) \in \mathbb{R}$ and $f(\mathbf{x}) \in \mathbb{R}^m$. The proof for the case where $f(\mathbf{x}) \in \mathbb{R}$ can be inferred from $f(\mathbf{x}) \in \mathbb{R}^m$. Therefore, we will only provide the proof for approximating $f(\mathbf{x}) \in \mathbb{R}^m$ using UAT.

Lemma 1. The mathematical form of UAT remains unchanged when multiplied by a matrix (constant).

$$\begin{aligned} G(\mathbf{x}) &= \beta \sum_{j=1}^N \alpha_j \sigma(\mathbf{W}_j^T \mathbf{x} + \theta_j) \\ &= \sum_{j=1}^N \beta \alpha_j \sigma(\mathbf{W}_j^T \mathbf{x} + \theta_j) \end{aligned} \quad (1)$$

Eq. (1) shows the representation of UAT multiplying a matrix. Let $\alpha_j = \beta \alpha_j$, and the result remains consistent with the original UAT mathematical form. Thus, it is proven that the mathematical form of UAT remains unchanged when multiplied by a matrix (constant).

Lemma 2. Let the general term of the network be written as: $\mathbf{x}'_{i+1} = (\mathbf{W}'_{i+1,1} \mathbf{x}'_i + \mathbf{b}'_{i+1,3}) + \mathbf{W}'_{i+1,3} \sigma(\mathbf{W}'_{i+1,2} \mathbf{x}'_i + \mathbf{b}'_{i+1,2})$, $i = 0, 1, 2, 3, \dots$. The multi-layer network of this form still corresponds to the mathematical form of UAT, and we refer to such a network as a residual network.

To prove that a multi-layer network with the general term written as $\mathbf{x}'_{i+1} = (\mathbf{W}'_{i+1,1} \mathbf{x}'_i + \mathbf{b}'_{i+1,3}) + \mathbf{W}'_{i+1,3} \sigma(\mathbf{W}'_{i+1,2} \mathbf{x}'_i + \mathbf{b}'_{i+1,2})$ corresponds to the UAT mathematical form, we first provide the forms of single-layer and two-layer networks, as shown in Eq. (2) and (3).

$$\mathbf{x}'_1 = (\mathbf{W}'_{1,1} \mathbf{x}'_0 + \mathbf{b}'_{1,3}) + \mathbf{W}'_{1,3} \sigma(\mathbf{W}'_{1,2} \mathbf{x}'_0 + \mathbf{b}'_{1,2}) \quad (2)$$

In Eq. (3), let $\mathbf{W}'_{2,1} = \frac{\mathbf{W}'_{2,1} \mathbf{W}'}{1,1}$, $\mathbf{b}'_{2,1} = \frac{\mathbf{W}'_{2,1} \mathbf{b}'_{1,3} + \mathbf{b}'_{2,3}}{1,1}$, $\mathbf{W}'_{1,3} = \frac{\mathbf{W}'_{2,1} \mathbf{W}'_{1,3}}{1,1}$, $\mathbf{W}'_{2,3} = \frac{\mathbf{W}'_{2,2} \mathbf{W}'_{1,1}}{1,1}$, and $\mathbf{b}'_{2,2} = \frac{(\mathbf{W}'_{2,2} \mathbf{b}'_{1,3} + \mathbf{b}'_{2,2}) + \mathbf{W}'_{2,2} \mathbf{W}'_{1,3} \sigma(\mathbf{W}'_{1,2} \mathbf{x}'_0 + \mathbf{b}'_{1,2})}{1,1}$. Thus, Eq. (4) can be written as:

$$\begin{aligned} \mathbf{x}'_2 &= (\mathbf{W}'_{2,1} \mathbf{x}'_0 + \mathbf{b}'_{2,1}) + \mathbf{W}'_{1,3} \sigma(\mathbf{W}'_{1,2} \mathbf{x}'_0 + \mathbf{b}'_{1,2}) \\ &\quad + \mathbf{W}'_{2,3} \sigma(\mathbf{W}'_{2,2} \mathbf{x}'_0 + \mathbf{b}'_{2,2}) \end{aligned} \quad (4)$$

Why can we combine the above terms? Because once the network training is complete, we know these parameters, so they can be directly calculated and thus combined. And $\mathbf{b}'_{2,2} = (\mathbf{W}'_{2,2} \mathbf{b}'_{1,3} + \mathbf{b}'_{2,2}) + \mathbf{W}'_{2,2} \mathbf{W}'_{1,3} \sigma(\mathbf{W}'_{1,2} \mathbf{x}'_0 + \mathbf{b}'_{1,2})$

clearly has the same mathematical form as UAT. We can understand it as dynamically fitting the bias term $\mathbf{b}'_{2,2}$ using UAT based on the input. Therefore, we have proven that the mathematical form of one and two-layer residual networks is consistent with the UAT mathematical form.

Assume that the mathematical form of the first i layers of the residual network is consistent with UAT. Our goal is to prove that the mathematical form of the $i+1$ -th layer of the residual network is still consistent with UAT. For convenience of expression, we make the following definition: since the mathematical form of the first i layers of the residual network is consistent with UAT, we write \mathbf{x}'_i as $\mathbf{x}'_i = (\mathbf{W}'_{i,1} \mathbf{x}'_0 + \mathbf{b}'_{i,1}) + UAT_i^R$, where the first term is written separately and the rest is written as the remainder term UAT_i^R . Since $\mathbf{x}'_{i+1} = (\mathbf{W}'_{i+1,1} \mathbf{x}'_i + \mathbf{b}'_{i+1,3}) + \mathbf{W}'_{i+1,3} \sigma(\mathbf{W}'_{i+1,2} \mathbf{x}'_i + \mathbf{b}'_{i+1,2})$, we divide \mathbf{x}'_{i+1} into two parts: $(\mathbf{W}'_{i+1,1} \mathbf{x}'_i + \mathbf{b}'_{i+1,3})$ and $\mathbf{W}'_{i+1,3} \sigma(\mathbf{W}'_{i+1,2} \mathbf{x}'_i + \mathbf{b}'_{i+1,2})$.

First, consider the part $(\mathbf{W}'_{i+1,1} \mathbf{x}'_i + \mathbf{b}'_{i+1,3})$. Substitute $\mathbf{x}'_i = (\mathbf{W}'_{i,1} \mathbf{x}'_0 + \mathbf{b}'_{i,1}) + UAT_i^R$ into it, and we get Eq. 5. Let $\mathbf{W}'_{i+1,1} = \frac{\mathbf{W}'_{i+1,1} \mathbf{W}'_{i,1}}{1,1}$ and $\mathbf{b}'_{i+1,1} = \frac{\mathbf{W}'_{i+1,1} \mathbf{b}'_{i,1} + \mathbf{b}'_{i+1,3}}{1,1}$, we can simplify the first part to $(\mathbf{W}'_{i+1,1} \mathbf{x}'_0 + \mathbf{b}'_{i+1,1}) + \mathbf{W}'_{i+1,1} UAT_i^R$. Since the mathematical form of UAT_i^R is consistent with UAT, and we have already proven that the mathematical form of UAT remains unchanged when multiplied by a matrix, we have proven that the mathematical form of the first part is consistent with UAT.

Next, we prove that the mathematical form of the second part, $\mathbf{W}'_{i+1,3} \sigma(\mathbf{W}'_{i+1,2} \mathbf{x}'_i + \mathbf{b}'_{i+1,2})$, is consistent with UAT. By substituting $\mathbf{x}'_i = (\mathbf{W}'_{i,1} \mathbf{x}'_0 + \mathbf{b}'_{i,1}) + UAT_i^R$ into it, we obtain Eq. (6). Let $\mathbf{W}'_{i+1,2} = \frac{\mathbf{W}'_{i+1,2} \mathbf{W}'_{i,1}}{1,1}$ and $\mathbf{b}'_{i+1,2} = \frac{(\mathbf{W}'_{i+1,2} \mathbf{b}'_{i,1} + \mathbf{b}'_{i+1,2}) + \mathbf{W}'_{i+1,2} UAT_i^R}{1,1}$. Thus, the second term can be written as $\mathbf{W}'_{i+1,3} \sigma(\mathbf{W}'_{i+1,2} \mathbf{x}'_0 + \mathbf{b}'_{i+1,2})$, which can be considered as a term within UAT. Here, $\mathbf{b}'_{i+1,2}$ is a bias term approximated using UAT.

Since the first term of \mathbf{x}'_{i+1} has the same mathematical form as UAT, and the second term can be considered as a component within UAT, the sum of both terms still corresponds to the UAT mathematical form. Therefore, we have proven that the mathematical form of a multi-layer residual network is consistent with the UAT mathematical form. The difference lies in that some bias terms are approximated using UAT rather than being directly defined.

A.2 The UAT Format of Residual-based CNNs

To demonstrate its relationship with UAT, we will provide its general form based on the definitions in Figure 8 in main text and then compare it with the general form presented in Section A.1: $\mathbf{x}'_{i+1} = (\mathbf{W}'_{i+1,1} \mathbf{x}'_i + \mathbf{b}'_{i+1,3}) + \mathbf{W}'_{i+1,3} \sigma(\mathbf{W}'_{i+1,2} \mathbf{x}'_i + \mathbf{b}'_{i+1,2})$. By examining the relation-

$$\begin{aligned}
\mathbf{x}'_2 &= \mathbf{W}'_{2,1}\mathbf{x}'_1 + \mathbf{W}'_{2,3}\sigma(\mathbf{W}'_{2,2}\mathbf{x}'_1 + \mathbf{b}'_{2,2}) + \mathbf{b}'_{2,3} \\
&= (\mathbf{W}'_{2,1}\mathbf{x}'_1 + \mathbf{b}'_{2,3}) + \mathbf{W}'_{2,3}\sigma(\mathbf{W}'_{2,2}\mathbf{x}'_1 + \mathbf{b}'_{2,2}) \\
&= \{\mathbf{W}'_{2,1}[(\mathbf{W}'_{1,1}\mathbf{x}'_0 + \mathbf{b}'_{1,3}) + \mathbf{W}'_{1,3}\sigma(\mathbf{W}'_{1,2}\mathbf{x}'_0 + \mathbf{b}'_{1,2})] + \mathbf{b}'_{2,3}\} \\
&\quad + \mathbf{W}'_{2,3}\sigma\{\mathbf{W}'_{2,2}[(\mathbf{W}'_{1,1}\mathbf{x}'_0 + \mathbf{b}'_{1,3}) + \mathbf{W}'_{1,3}\sigma(\mathbf{W}'_{1,2}\mathbf{x}'_0 + \mathbf{b}'_{1,2})] + \mathbf{b}'_{2,2}\} \\
&= \{\mathbf{W}'_{2,1}(\mathbf{W}'_{1,1}\mathbf{x}'_0 + \mathbf{b}'_{1,3}) + \mathbf{b}'_{2,3} + \mathbf{W}'_{2,1}\mathbf{W}'_{1,3}\sigma(\mathbf{W}'_{1,2}\mathbf{x}'_0 + \mathbf{b}'_{1,2})\} \\
&\quad + \mathbf{W}'_{2,3}\sigma\{\mathbf{W}'_{2,2}(\mathbf{W}'_{1,1}\mathbf{x}'_0 + \mathbf{b}'_{1,3}) + \mathbf{b}'_{2,2} + \mathbf{W}'_{2,2}\mathbf{W}'_{1,3}\sigma(\mathbf{W}'_{1,2}\mathbf{x}'_0 + \mathbf{b}'_{1,2})\} \\
&= \{(\mathbf{W}'_{2,1}\mathbf{W}'_{1,1}\mathbf{x}'_0 + \mathbf{W}'_{2,1}\mathbf{b}'_{1,3} + \mathbf{b}'_{2,3}) + \mathbf{W}'_{2,1}\mathbf{W}'_{1,3}\sigma(\mathbf{W}'_{1,2}\mathbf{x}'_0 + \mathbf{b}'_{1,2})\} \\
&\quad + \mathbf{W}'_{2,3}\sigma\{\mathbf{W}'_{2,2}\mathbf{W}'_{1,1}\mathbf{x}'_0 + (\mathbf{W}'_{2,2}\mathbf{b}'_{1,3} + \mathbf{b}'_{2,2}) + \mathbf{W}'_{2,2}\mathbf{W}'_{1,3}\sigma(\mathbf{W}'_{1,2}\mathbf{x}'_0 + \mathbf{b}'_{1,2})\}
\end{aligned} \tag{3}$$

$$\begin{aligned}
&(\mathbf{W}'_{i+1,1}\mathbf{x}'_i + \mathbf{b}'_{i+1,3}) \\
&= \{\mathbf{W}'_{i+1,1}[(\mathbf{W}'_{i,1}\mathbf{x}'_0 + \mathbf{b}'_{i,1}) + UAT_i^R] + \mathbf{b}'_{i+1,3}\} \\
&= \{\mathbf{W}'_{i+1,1}(\mathbf{W}'_{i,1}\mathbf{x}'_0 + \mathbf{b}'_{i,1}) + \mathbf{W}'_{i+1,1}UAT_i^R + \mathbf{b}'_{i+1,3}\} \\
&= \{[\mathbf{W}'_{i+1,1}\mathbf{W}'_{i,1}\mathbf{x}'_0 + (\mathbf{W}'_{i+1,1}\mathbf{b}'_{i,1} + \mathbf{b}'_{i+1,3})] + \mathbf{W}'_{i+1,1}UAT_i^R\}
\end{aligned} \tag{5}$$

$$\begin{aligned}
&\mathbf{W}'_{i+1,3}\sigma(\mathbf{W}'_{i+1,2}\mathbf{x}'_i + \mathbf{b}'_{i+1,2}) \\
&= \mathbf{W}'_{i+1,3}\sigma\{\mathbf{W}'_{i+1,2}[(\mathbf{W}'_{i,1}\mathbf{x}'_0 + \mathbf{b}'_{i,1}) + UAT_i^R] + \mathbf{b}'_{i+1,2}\} \\
&= \mathbf{W}'_{i+1,3}\sigma\{\mathbf{W}'_{i+1,2}(\mathbf{W}'_{i,1}\mathbf{x}'_0 + \mathbf{b}'_{i,1}) + \mathbf{W}'_{i+1,2}UAT_i^R + \mathbf{b}'_{i+1,2}\} \\
&= \mathbf{W}'_{i+1,3}\sigma\{\mathbf{W}'_{i+1,2}\mathbf{W}'_{i,1}\mathbf{x}'_0 + (\mathbf{W}'_{i+1,2}\mathbf{b}'_{i,1} + \mathbf{b}'_{i+1,2}) + \mathbf{W}'_{i+1,2}UAT_i^R\}
\end{aligned} \tag{6}$$

ship between these two forms, we can prove that the mathematical form of a multi-layer residual-based convolutional network is consistent with the UAT. The general term of residual-based CNNs is shown in Eq. (7)

$$\begin{aligned}
\mathbf{x}'_{i+1} &= \mathbf{x}'_i + \mathbf{W}'_{i+1,2}\sigma(\mathbf{W}'_{i+1,1}\mathbf{x}'_i + \mathbf{b}_{i+1,1}) + \mathbf{b}_{i+1,2} \\
&= (\mathbf{x}'_i + \mathbf{b}_{i+1,2}) + \mathbf{W}'_{i+1,2}\sigma(\mathbf{W}'_{i+1,1}\mathbf{x}'_i + \mathbf{b}_{i+1,1})
\end{aligned} \tag{7}$$

Compared to $\mathbf{x}'_{i+1} = (\mathbf{W}'_{i+1,1}\mathbf{x}'_i + \mathbf{b}'_{i+1,3}) + \mathbf{W}'_{i+1,3}\sigma(\mathbf{W}'_{i+1,2}\mathbf{x}'_i + \mathbf{b}'_{i+1,2})$, the only difference lies in $\mathbf{W}'_{i+1,1}\mathbf{x}'_i + \mathbf{b}'_{i+1,3}$. It is easy to deduce that the presence or absence of $\mathbf{W}'_{i+1,1}$ does not affect the overall mathematical form. Therefore, residual-based CNNs are also concrete implementations of the UAT. To clearly present the UAT format, we will use the method mentioned in Section A.1. Assuming the mathematical form of \mathbf{x}'_i is consistent with UAT, we decompose \mathbf{x}'_i into a primary term plus a remainder term, written as $\mathbf{x}'_i = (\mathbf{x}_0 + \mathbf{b}_{i,2}) + UAT_i^R$. Substituting this into $(\mathbf{x}'_i + \mathbf{b}_{i+1,2}) + \mathbf{W}'_{i+1,2}\sigma(\mathbf{W}'_{i+1,1}\mathbf{x}'_i + \mathbf{b}_{i+1,1})$, we obtain Eq. (9). Setting $\mathbf{b}_{i+1,2} = \mathbf{b}_{i,2} + \mathbf{b}_{i+1,2}$ and $\mathbf{b}_{i+1,1} = (\mathbf{W}'_{i+1,1}\mathbf{b}_{i,1} + \mathbf{b}_{i+1,1}) + \mathbf{W}'_{i+1,1}UAT_i^R$, we finally get $\mathbf{x}_{i+1} = (\mathbf{x}_0 + \mathbf{b}_{i+1,2}) + UAT_i^R + \mathbf{W}'_{i+1,2}\sigma(\mathbf{W}'_{i+1,1}\mathbf{x}_0 + \mathbf{b}_{i+1,1})$. Since the mathematical form of UAT_i^R is consistent with multi-layer UAT, it follows that multi-layer residual CNNs are also specific implementations of UAT. In addition,

$UAT_{i+1} = UAT_i^R + \mathbf{W}'_{i+1,2}\sigma(\mathbf{W}'_{i+1,1}\mathbf{x}_0 + \mathbf{b}_{i+1,1})$. So, $\mathbf{x}_{i+1} = (\mathbf{x}_0 + \mathbf{b}_{i+1,2}) + UAT_{i+1}$, where $UAT_{i+1} = \sum_{j=1}^{i+1} \mathbf{W}'_{j,2}\sigma(\mathbf{W}'_{j,1}\mathbf{x}_0 + \mathbf{b}'_{j,1})$, $\mathbf{b}'_{j,1} = (\mathbf{W}'_{j,1}\mathbf{b}'_{j-1,2} + \mathbf{b}'_{j,1}) + \mathbf{W}'_{j,1}UAT_{j-1}$. In conclusion, the UAT format of $i+1$ -layer residual-based CNN is:

$$\mathbf{x}'_{i+1} = (\mathbf{x}_0 + \mathbf{b}'_{i+1,2}) + \sum_{j=1}^{i+1} \mathbf{W}'_{j,2}\sigma(\mathbf{W}'_{j,1}\mathbf{x}_0 + \mathbf{b}'_{j,1}) \tag{8}$$

$\mathbf{b}'_{j,1}$ is a j -layer UAT and the input is \mathbf{x}_0 . Of course, aside from the parameter $\mathbf{b}'_{j,1}$, which changes as the number of layers increases, other parameters will also vary with the number of layers. However, as demonstrated in the above derivation, these changes involve only matrix multiplications or additions. Thus, they do not fundamentally alter the mathematical form of the UAT. Therefore, we will not detail the specific forms of them here. But we provide some examples in Figure 1

A.3 The UAT Format of Transformer-based ViTs

Similarly, To illustrate its relationship with the UAT, we will first derive the general form based on Figure 9 in main text and then compare it with the general form given in Section A.1: $\mathbf{x}'_{i+1} = (\mathbf{W}'_{i+1,1}\mathbf{x}'_i + \mathbf{b}'_{i+1,3}) + \mathbf{W}'_{i+1,3}\sigma(\mathbf{W}'_{i+1,2}\mathbf{x}'_i + \mathbf{b}'_{i+1,2})$.

By examining the relationship between these forms, we can demonstrate that the mathematical form of multi-layer

$$\begin{aligned}
& (\mathbf{x}'_i + \mathbf{b}_{i+1,2}) + \mathbf{W}'_{i+1,2}\sigma(\mathbf{W}'_{i+1,1}\mathbf{x}'_i + \mathbf{b}_{i+1,1}) \\
& = [(\mathbf{x}_0 + \mathbf{b}_{i,1}) + UAT_i^R + \mathbf{b}_{i+1,2}] + \mathbf{W}'_{i+1,2}\sigma\{\mathbf{W}'_{i+1,1}[(\mathbf{x}_0 + \mathbf{b}_{i,1}) + UAT_i^R] + \mathbf{b}_{i+1,1}\} \\
& = (\mathbf{x}_0 + \underline{\mathbf{b}_{i,1} + \mathbf{b}_{i+1,2}}) + UAT_i^R + \mathbf{W}'_{i+1,2}\sigma\{\mathbf{W}'_{i+1,1}\mathbf{x}_0 + (\mathbf{W}'_{i+1,1}\mathbf{b}_{i,1} + \mathbf{b}_{i+1,1}) + \mathbf{W}'_{i+1,1}UAT_i^R\}
\end{aligned} \tag{9}$$

$\mathbf{x}'_1 = (\mathbf{x}'_0 + \mathbf{b}_{1,2}) + \mathbf{W}'_{1,2}\sigma(\mathbf{W}'_{1,1}\mathbf{x}'_0 + \mathbf{b}_{1,1})$	$\mathbf{x}'_1 = (\mathbf{x}'_0 + \mathbf{b}_{1,2}) + UAT_1^R$	$UAT_1^R = \mathbf{W}'_{1,2}\sigma(\mathbf{W}'_{1,1}\mathbf{x}'_0 + \mathbf{b}_{1,1})$
$\mathbf{x}'_2 = (\mathbf{x}'_0 + \mathbf{b}_{2,2}) + \mathbf{W}'_{1,2}\sigma(\mathbf{W}'_{1,1}\mathbf{x}'_0 + \mathbf{b}_{1,1}) + \mathbf{W}'_{2,2}\sigma(\mathbf{W}'_{2,1}\mathbf{x}'_0 + \mathbf{b}_{2,1})$	$\mathbf{x}'_2 = (\mathbf{x}'_0 + \mathbf{b}_{2,2}) + UAT_2^R$	$UAT_2^R = \mathbf{W}'_{1,2}\sigma(\mathbf{W}'_{1,1}\mathbf{x}'_0 + \mathbf{b}_{1,1}) + \mathbf{W}'_{2,2}\sigma(\mathbf{W}'_{2,1}\mathbf{x}'_0 + \mathbf{b}_{2,1})$
$\mathbf{b}_{2,2} = \mathbf{b}_{1,2} + \mathbf{b}_{2,2}$ $\mathbf{b}_{2,1} = (\mathbf{W}'_{2,1}\mathbf{b}_{1,2} + \mathbf{b}_{2,1}) + \mathbf{W}'_{2,1}\mathbf{W}'_{1,2}\sigma(\mathbf{W}'_{1,1}\mathbf{x}'_0 + \mathbf{b}_{1,1})$		
$\mathbf{x}'_3 = (\mathbf{x}'_0 + \mathbf{b}_{3,2}) + \mathbf{W}'_{1,2}\sigma(\mathbf{W}'_{1,1}\mathbf{x}'_0 + \mathbf{b}_{1,1}) + \mathbf{W}'_{2,2}\sigma(\mathbf{W}'_{2,1}\mathbf{x}'_0 + \mathbf{b}_{2,1}) + \mathbf{W}'_{3,2}\sigma(\mathbf{W}'_{3,1}\mathbf{x}'_0 + \mathbf{b}_{3,1})$	$\mathbf{x}'_3 = (\mathbf{x}'_0 + \mathbf{b}_{3,2}) + UAT_3^R$	$UAT_3^R = \mathbf{W}'_{1,2}\sigma(\mathbf{W}'_{1,1}\mathbf{x}'_0 + \mathbf{b}_{1,1}) + \mathbf{W}'_{2,2}\sigma(\mathbf{W}'_{2,1}\mathbf{x}'_0 + \mathbf{b}_{2,1}) + \mathbf{W}'_{3,2}\sigma(\mathbf{W}'_{3,1}\mathbf{x}'_0 + \mathbf{b}_{3,1})$
$\mathbf{b}_{3,2} = \mathbf{b}_{2,2} + \mathbf{b}_{3,2}$ $\mathbf{b}_{3,1} = (\mathbf{W}'_{3,1}\mathbf{b}_{2,2} + \mathbf{b}_{3,1}) + \mathbf{W}'_{3,1}\mathbf{W}'_{1,2}\sigma(\mathbf{W}'_{1,1}\mathbf{x}'_0 + \mathbf{b}_{1,1}) + \mathbf{W}'_{3,1}\mathbf{W}'_{2,2}\sigma(\mathbf{W}'_{2,1}\mathbf{x}'_0 + \mathbf{b}_{2,1})$		
\vdots	\vdots	\vdots

Figure 1: Some examples of the UAT format of multi-layer residual-based convolution. The changes of parameters are represented within the dashed boxes. The parameters on the right of the equations indicate the original values, while those on the left represent the transformed values. There is no specific order of calculation for the parameters within each dashed box, but there is a top-to-bottom calculation order between different dashed boxes.

Transformer networks is consistent with the UAT. The Transformer involves two key operations: multi-head attention (MHA) and feed-forward networks (FFN). These operations, when expressed in matrix-vector form, correspond to Eq.(10) and Eq.(11), respectively. Consequently, the general term for a Transformer-based network can be written as Eq. (12).

$$MHA(\mathbf{x}'_i) = \mathbf{W}'_{i,1}\mathbf{x}'_i \tag{10}$$

$$FFN(\mathbf{x}'_i) = \mathbf{W}'_{i,3}\sigma(\mathbf{W}'_{i,2}\mathbf{x}'_i + \mathbf{b}'_{i,2}) + \mathbf{b}'_{i,3} \tag{11}$$

Let $\mathbf{W}'_{i+1,2} = \mathbf{W}'_{i+1,2}\mathbf{W}'_{i+1,1}$, so we have $\mathbf{x}'_{i+1} = (\mathbf{W}'_{i+1,1}\mathbf{x}'_i + \mathbf{b}'_{i+1,3}) + \mathbf{W}'_{i,3}\sigma(\mathbf{W}'_{i+1,2}\mathbf{x}'_i + \mathbf{b}'_{i+1,2})$. It is evident that, when compared to the general form given in Section A.1: $\mathbf{x}'_{i+1} = (\mathbf{W}'_{i+1,1}\mathbf{x}'_i + \mathbf{b}'_{i+1,3}) + \mathbf{W}'_{i+1,3}\sigma(\mathbf{W}'_{i+1,2}\mathbf{x}'_i + \mathbf{b}'_{i+1,2})$, the mathematical forms are the same. Therefore, multi-layer Transformers are also specific implementations of the UAT. Similarly, to clearly present the UAT format, we use the method mentioned in Section A.1. Assuming the mathematical form of \mathbf{x}'_i is consistent with UAT, we decompose \mathbf{x}'_i

into a primary term plus a remainder term, written as $\mathbf{x}'_i = (\mathbf{W}'_{i,1}\mathbf{x}_0 + \mathbf{b}_{i,3}) + UAT_i^R$. Substituting this into $\mathbf{x}'_{i+1} = (\mathbf{W}'_{i+1,1}\mathbf{x}'_i + \mathbf{b}'_{i+1,3}) + \mathbf{W}'_{i,3}\sigma(\mathbf{W}'_{i+1,2}\mathbf{x}'_i + \mathbf{b}'_{i+1,2})$, we obtain Eq. (14). By setting $\mathbf{W}'_{i+1,1} = \mathbf{W}'_{i+1,1}\mathbf{W}_{i,1}$, $\mathbf{b}'_{i+1,3} = (\mathbf{W}'_{i+1,1}\mathbf{b}_{i,1} + \mathbf{b}'_{i+1,3})$, $UAT_i^R = \mathbf{W}'_{i+1,1}UAT_i^R$, and $\mathbf{W}'_{i+1,2} = \mathbf{W}'_{i+1,2}\mathbf{W}_{i,1}$, $\mathbf{b}'_{i+1,2} = (\mathbf{W}'_{i+1,2}\mathbf{b}_{i,1} + \mathbf{b}'_{i+1,2}) + \mathbf{W}'_{i+1,2}UAT_i^R$, we get $\mathbf{x}'_{i+1} = (\mathbf{W}'_{i+1,1}\mathbf{x}_0 + \mathbf{b}'_{i+1,3}) + UAT_i^R + \mathbf{W}'_{i,3}\sigma(\mathbf{W}'_{i+1,2}\mathbf{x}_0 + \mathbf{b}'_{i+1,2})$. Since the mathematical form of UAT_i^R is consistent with multi-layer UAT, it follows that multi-layer Transformer networks are also specific implementations of UAT. In addition, $UAT_{i+1}^R = UAT_i^R + \mathbf{W}'_{i+1,3}\sigma(\mathbf{W}'_{i+1,2}\mathbf{x}_0 + \mathbf{b}'_{i+1,2})$. So, $\mathbf{x}_{i+1} = (\mathbf{W}'_{i+1,1}\mathbf{x}_0 + \mathbf{b}_{i+1,3}) + UAT_{i+1}^R$, where $i = 0, 1, 2, \dots$, $UAT_{i+1}^R = \sum_{j=1}^{i+1} \mathbf{W}'_{j,3}\sigma(\mathbf{W}'_{j,2}\mathbf{x}_0 + \mathbf{b}'_{j,2})$, $\mathbf{b}'_{j,2} = (\mathbf{W}'_{j,2}\mathbf{b}'_{j-1,3} + \mathbf{b}'_{j,2}) + \mathbf{W}'_{j,2}UAT_{j-1}^R$. To sum up, the $i+1$ -layer Transformer can be written as:

$$\mathbf{x}_{i+1} = (\mathbf{W}'_{i+1,1}\mathbf{x}_0 + \mathbf{b}_{i+1,1}) + \sum_{j=1}^{i+1} \mathbf{W}'_{j,3}\sigma(\mathbf{W}'_{j,2}\mathbf{x}_0 + \mathbf{b}'_{j,2}) \tag{13}$$

$$\begin{aligned}
\mathbf{x}'_{i+1} &= \mathbf{W}'_{i+1,1}\mathbf{x}'_i + \mathbf{W}'_{i+1,3}\sigma[\mathbf{W}'_{i+1,2}(\mathbf{W}'_{i+1,1}\mathbf{x}'_i) + \mathbf{b}'_{i+1,2}] + \mathbf{b}'_{i+1,3} \\
&= \mathbf{W}'_{i+1,1}\mathbf{x}'_i + \mathbf{W}'_{i+1,3}\sigma(\underline{\mathbf{W}'_{i+1,2}\mathbf{W}'_{i+1,1}\mathbf{x}'_i} + \mathbf{b}'_{i+1,2}) + \mathbf{b}'_{i+1,3}
\end{aligned} \tag{12}$$

The same to residual-based CNNs, other parameters will also vary with the number of layers. And, these changes involve only matrix multiplications or additions. Thus, they do not fundamentally alter the mathematical form of the UAT. Therefore, we will not detail the specific forms for each layer here.

The biggest difference between Transformers and CNNs lies in the fact that the parameters in the Multi-Head Attention (MHA) mechanism dynamically change with the input. Therefore, in the corresponding UAT mathematical form for Transformers, all $\mathbf{W}'_{j,1}$ and $\mathbf{W}'_{j,2}$ parameters for the i -th layer, where $j = 1, \dots, i$, are dynamically changing with the input. We give some examples in Figure 2.

$$\begin{aligned}
\mathbf{x}'_{i+1} &= (\mathbf{W}'_{i+1,1}\mathbf{x}'_i + \mathbf{b}'_{i+1,3}) + \mathbf{W}'_{i,3}\sigma(\mathbf{W}'_{i+1,2}\mathbf{x}'_i + \mathbf{b}'_{i+1,2}) \\
&= \{\mathbf{W}'_{i+1,1}[(\mathbf{W}_{i,1}\mathbf{x}_0 + \mathbf{b}_{i,1}) + UAT_i^R] + \mathbf{b}'_{i+1,3}\} \\
&\quad + \mathbf{W}'_{i,3}\sigma\{\mathbf{W}'_{i+1,2}[(\mathbf{W}_{i,1}\mathbf{x}_0 + \mathbf{b}_{i,1}) + UAT_i^R] + \mathbf{b}'_{i+1,2}\} \\
&= [\underline{\mathbf{W}'_{i+1,1}\mathbf{W}_{i,1}\mathbf{x}_0} + \underline{(\mathbf{W}'_{i+1,1}\mathbf{b}_{i,1} + \mathbf{b}'_{i+1,3})} + \underline{\mathbf{W}'_{i+1,1}UAT_i^R}] \\
&\quad + \mathbf{W}'_{i,3}\sigma\{\underline{\mathbf{W}'_{i+1,2}\mathbf{W}_{i,1}\mathbf{x}_0} + \underline{(\mathbf{W}'_{i+1,2}\mathbf{b}_{i,1} + \mathbf{b}'_{i+1,2})} + \underline{\mathbf{W}'_{i+1,2}UAT_i^R}\}
\end{aligned} \tag{14}$$

$ \begin{aligned} \mathbf{x}'_1 &= (\mathbf{W}'_{1,1}\mathbf{x}'_0 + \mathbf{b}'_{1,3}) + \mathbf{W}'_{1,3}\sigma(\mathbf{W}'_{1,2}\mathbf{x}'_0 + \mathbf{b}'_{1,2}) \\ &\quad \boxed{\mathbf{W}_{1,2} = \mathbf{W}'_{1,2}\mathbf{W}'_{1,1}} \end{aligned} $	$ \mathbf{x}'_1 = (\mathbf{W}_{1,1}\mathbf{x}'_0 + \mathbf{b}_{1,3}) + UAT_1^R $	$ UAT_1^R = \mathbf{W}'_{1,3}\sigma(\mathbf{W}'_{1,2}\mathbf{x}'_0 + \mathbf{b}'_{1,2}) $
$ \begin{aligned} \mathbf{x}'_2 &= (\mathbf{W}'_{2,1}\mathbf{x}'_0 + \mathbf{b}'_{2,3}) + \mathbf{W}'_{1,3}\sigma(\mathbf{W}'_{1,2}\mathbf{x}'_0 + \mathbf{b}'_{1,2}) \\ &\quad + \mathbf{W}'_{2,3}\sigma(\mathbf{W}'_{2,2}\mathbf{x}'_0 + \mathbf{b}'_{2,2}) \\ &\quad \boxed{\mathbf{W}'_{2,1} = \mathbf{W}'_{2,1}\mathbf{W}'_{1,1}} \\ &\quad \boxed{\mathbf{b}'_{2,3} = \mathbf{W}'_{2,1}\mathbf{b}'_{1,3} + \mathbf{b}'_{2,3}} \\ &\quad \boxed{\mathbf{W}'_{1,3} = \mathbf{W}'_{2,1}\mathbf{W}'_{1,3}} \\ &\quad \boxed{\mathbf{W}'_{2,2} = \mathbf{W}'_{2,2}\mathbf{W}'_{1,1}} \\ &\quad \boxed{\mathbf{b}'_{2,2} = (\mathbf{W}'_{2,2}\mathbf{b}'_{1,3} + \mathbf{b}'_{2,2}) + \mathbf{W}'_{2,2}\mathbf{W}'_{1,3}\sigma(\mathbf{W}'_{1,2}\mathbf{x}'_0 + \mathbf{b}'_{1,2})} \\ &\quad \boxed{\dots} \end{aligned} $	$ \mathbf{x}'_2 = (\mathbf{W}'_{2,1}\mathbf{x}'_0 + \mathbf{b}'_{2,3}) + UAT_2^R $	$ UAT_2^R = \mathbf{W}'_{1,3}\sigma(\mathbf{W}'_{1,2}\mathbf{x}'_0 + \mathbf{b}'_{1,2}) \\ + \mathbf{W}'_{2,3}\sigma(\mathbf{W}'_{2,2}\mathbf{x}'_0 + \mathbf{b}'_{2,2}) $
$ \begin{aligned} \mathbf{x}'_3 &= (\mathbf{W}'_{3,1}\mathbf{x}'_0 + \mathbf{b}'_{3,3}) + \mathbf{W}'_{1,3}\sigma(\mathbf{W}'_{1,2}\mathbf{x}'_0 + \mathbf{b}'_{1,2}) \\ &\quad + \mathbf{W}'_{2,3}\sigma(\mathbf{W}'_{2,2}\mathbf{x}'_0 + \mathbf{b}'_{2,2}) + \mathbf{W}'_{3,3}\sigma(\mathbf{W}'_{3,2}\mathbf{x}'_0 + \mathbf{b}'_{3,2}) \\ &\quad \boxed{\mathbf{W}'_{3,1} = \mathbf{W}'_{3,1}\mathbf{W}'_{2,1}} \\ &\quad \boxed{\mathbf{b}'_{3,3} = \mathbf{W}'_{3,1}\mathbf{b}'_{2,3} + \mathbf{b}'_{3,3}} \\ &\quad \boxed{\mathbf{W}'_{1,3} = \mathbf{W}'_{3,1}\mathbf{W}'_{1,3}} \\ &\quad \boxed{\mathbf{W}'_{2,3} = \mathbf{W}'_{3,1}\mathbf{W}'_{2,3}} \\ &\quad \boxed{\mathbf{W}'_{3,2} = \mathbf{W}'_{3,2}\mathbf{W}'_{2,1}} \\ &\quad \boxed{\mathbf{b}'_{3,2} = (\mathbf{W}'_{3,2}\mathbf{b}'_{2,3} + \mathbf{b}'_{3,2}) + \mathbf{W}'_{3,2}\mathbf{W}'_{1,3}\sigma(\mathbf{W}'_{1,2}\mathbf{x}'_0 + \mathbf{b}'_{1,2})} \\ &\quad + \mathbf{W}'_{3,2}\mathbf{W}'_{2,3}\sigma(\mathbf{W}'_{2,2}\mathbf{x}'_0 + \mathbf{b}'_{2,2}) \\ &\quad \boxed{\dots} \end{aligned} $	$ \mathbf{x}'_3 = (\mathbf{W}'_{3,1}\mathbf{x}'_0 + \mathbf{b}'_{3,3}) + UAT_3^R $	$ UAT_3^R = \mathbf{W}'_{1,3}\sigma(\mathbf{W}'_{1,2}\mathbf{x}'_0 + \mathbf{b}'_{1,2}) \\ + \mathbf{W}'_{2,3}\sigma(\mathbf{W}'_{2,2}\mathbf{x}'_0 + \mathbf{b}'_{2,2}) \\ + \mathbf{W}'_{3,3}\sigma(\mathbf{W}'_{3,2}\mathbf{x}'_0 + \mathbf{b}'_{3,2}) $
$ \begin{aligned} &\bullet \\ &\bullet \\ &\bullet \end{aligned} $	$ \begin{aligned} &\bullet \\ &\bullet \\ &\bullet \end{aligned} $	$ \begin{aligned} &\bullet \\ &\bullet \end{aligned} $

Figure 2: Some examples of the UAT format of multi-layer Transformer. The changes of parameters are represented within the dashed boxes. The parameters on the right of the equations indicate the original values, while those on the left represent the transformed values. There is no specific order of calculation for the parameters within each dashed box, but there is a top-to-bottom calculation order between different dashed boxes.